UK UNLIMITED

Procurement Executive - Ministry of Defence

AWRE, Aldermaston

(14) AWRE-O-21/80

(11) Jul 80

AWRE REPORT NO. O21/80

(6) Modelling of Compressed Magnetic Field Generators by Equivalent Circuit Approach

(10) M Jones

(18) DRIC

(19) BR-75017

(12) 54

Recommended for issue by

P F A Richards, Superintendent

Approved by

F E Whiteway, Head of Division

046650

ISBN 0 85518141 9

CONTENTS

SUMMARY

An equivalent circuit model is presented for a helical compressed magnetic field generator. The emphasis has been placed on producing a model which has a short computer run time.

Magnetic energy losses due to non-linear field diffusion are taken into account, together with the effects of magnetically-induced conductor motion.

Examples of the computer code results are given, together with a comparison with experimental data.

1. INTRODUCTION

The amplification of magnetic fields due to the driving of current carrying conductors at high velocities has found a number of applications. For instance, the high energy densities obtainable have been used to heat plasmas. Alternatively, the corresponding amplification of the current in the associated conductors serves as the basis for electrical energy generation in low impedance loads. The author is mainly concerned with this latter application.

In order to transduce significant quantities of electrical energy large conductor velocities are necessary. Too small a velocity leads to large diffusion losses resulting in a poor or even to an absence of energy gain. Conductors can be accelerated to substantial velocities by subjecting them to explosive impulse. Modern explosive technology permits controlled and repeatable experimentation in this area.

The helical generator allows one to conveniently match the device to the load and is the class of generator under consideration here. Such a device is shown schematically in figure 1. It consists of a cylindrical conducting shell

(armature) containing a high explosive together with a concentric helical coil. The generator is primed (given an initial current/field) by discharging a capacitor into the coil. Synchronised initiation of the explosive charge at one end leads to a funnelling of the armature and the trapping of magnetic flux between the armature and coil. The expanding armature systematically wipes out the space between the armature and coil leading to field, current and magnetic energy amplification. With suitable generator design, the transduced energy can be efficiently coupled into the load.

Because of its dependence on explosive technology the generator is of a "one shot" nature. However, this disadvantage is offset by the generator's ability to transduce substantial quantities of electrical energy at small volume. Nevertheless, because of the destructive nature of the experiments, generator development can be time-consuming and expensive. A realistic model represents an invaluable tool for minimising the time and cost of development. The model should ideally be capable of identifying the significance of the generator's parameters with a view to carrying out optimisation and sensitivity analyses. As a result, the experimental programme is minimised.

In order to be effective, the model should be capable of dealing with the essential physics of the generator. However, too rigorous a mathematical treatment of this coupled magneto-hydrodynamic problem leads to very lengthy computer calculations. Such treatments have been known to result in calculation times of many hours. Although giving greater exactness, these models tend to be of more limited use in parametric studies which entail large numbers of calculations. The approach presented here aims at producing a model containing all the essential physics while still maintaining a reasonably fast computer capability.

The two output characteristics of the generator which are of most interest are its amplification factors:-

$$\text{Current gain} = \frac{\text{peak generated current}}{\text{initial current}}.$$

$$\text{Energy gain} = \frac{\text{peak generated load magnetic energy}}{\text{initial magnetic energy}}.$$

The physical generator design may vary from that shown schematically in figure 1. For instance, in order to shorten the pulse shape the explosive charge may be initiated simultaneously at both ends (armature funnels in from both ends) or initiated at the mid-point (armature funnels towards both ends). The shortening of the running time does not lead to an enhancement of the amplification factors.

There are two distinct phases in the generator's operation. The initial phase involves the conversion of explosive energy into kinetic energy of the armature. This kinetic energy is then transduced into magnetic energy by virtue of the current carrying conductor doing work on the electromagnetic forces present. The high energy density of explosives represents the key to the generator's potential. However, the efficiency of conversion of kinetic to magnetic energy decreases with decreasing size of the generator because of the more severe diffusion and joule heating losses associated with small generators. In larger systems high efficiencies resulting from a total transfer of armature kinetic energy (turnaround) are achievable.

The model described in this report deals with fixed diameter (wire) round wire constant pitch helical coils only. In general as generators are scaled up in size and are run at higher energy levels, coils are graded in order to reduce losses due to joule heating and magnetic pressure effects (ie, wire diameter and pitch increase towards output end).

A previous description of this model has been given in reference (1).

2. THE BASIC GENERATOR MODEL

This takes the form of a lumped equivalent electrical circuit and is shown in figure 2. Magnetic energy stored in the generator between the coil and armature is continually being lost through the vacuum/conductor interface to be stored as magnetic energy in the conductor or dissipated as joule heat. This loss through the interface can be represented by effective resistances in the equivalent circuit (appendix A).

The circuit relation is

$$\frac{d}{dt}(LI) + RI = 0,$$

with solution at time t

$$\frac{I(t)}{I(o)} = \frac{L(o)}{L(t)} \exp\left\{-\int_o^t \frac{R}{L}(t)dt\right\}.$$

L and R refer to total circuit values and t = 0 refers to the priming condition.

2.1 Generator inductance

This is a circuit representation for the energy stored between the armature and coil. Standard techniques for calculating coil self and mutual inductances are given in reference (2). The geometry of figure 1 can be represented by a coil of given length and effective radius, the latter being based on the mean cross-sectional area between the armature and coil. Alternatively, the coil can be considered as a number of interacting sections. Further, the corresponding armature sections represent mirror images of the coil sections, ie, the coil sections and armature sections have similar ampere X turn values. In this case we have

$$L_g = \sum_{i=1}^{N} L_i + \sum_{k\neq i}^{N} \sum_{i=1}^{N} M_{ik} - \sum_{k=1}^{N} \sum_{i=1}^{M} m_{ik},$$

where the self-inductances of the coil sections are

$$L_i \quad i = 1, 2 \ldots\ldots N,$$

the mutual inductances between coil sections are

$$M_{ik} \quad i,k = 1, 2 \ldots\ldots N,$$

and the mutual inductances between coil/armature sections are

$$m_{ik} \quad i = 1, 2 \ldots\ldots N \; k = 1, 2 \ldots\ldots M.$$

2.2 Armature effective resistance

Because skin depths are in general much smaller than armature radial dimensions for the systems under consideration, a one-dimensional field diffusion problem is appropriate. The expression for the effective resistance is given in appendix A as

$$R_a = -\frac{n^2}{H_s^2}\int_s \rho H \frac{\partial H}{\partial x} dS, \qquad \ldots.(1)$$

where n is the coil winding density,

H_s is the magnetic field at the armature surface,

ρ is the material resistivity,

x is the distance measured into the conductor,

S is the armature surface area.

Hence, R_s is evaluated from a knowledge of the surface field and its gradient and the surface temperature which defines ρ. The surface field is given by

$$H_s = nI.$$

During the earlier part of the operation the armature consists of two sections having differing physical conditions, ie, shocked and pre-shocked conductors. In general, significant conductor heating occurs through joule dissipation and the problem is non-linear.

Three methods are employed to evaluate R_s. Two are based on exponential approximations for the current (and field) time profiles. The third represents a finite difference technique for arbitrary surface profile.

2.2.1 Equivalent skin depth method

The approach is similar to that of reference (3).

The solution of the linear field diffusion equation

$$\mu_o \partial H/\partial t = \rho \partial^2 H/\partial x^2$$

is for the case of an exponential applied surface field profile of form

$$H_s = H_o \exp(\alpha t)$$

with boundary condition $H(d,t) = 0$, where d is the conductor thickness.

$$H(x,t) = H_s \left[A \exp(-x/a) + (1 - A) \exp(x/a)\right] \quad \ldots.(2)$$

once the initial field profile H(x,o) has been overriden.

Where $a = \left(\frac{\rho}{\mu_o \alpha}\right)^{\frac{1}{2}}$ is the exponential skin depth,

μ_o is the conductor permeability.

$A = \left[1 - \exp(-2d/a)\right]^{-1}$.

Substitution of equation (2) in equation (1) gives

$$R_a = \frac{n^2 \rho (2A - 1)}{a} S.$$

The joule deposition in the conductor is given by

$$W_j = \frac{1}{2} I^2 R_e k',$$

where $R_e = \frac{n^2 \rho S}{a}$ and $k' = \left[2A - 1 - 4A(1 - A)^d/a\right]$.

We now make the approximation (3) that for $a \ll d$ the mean effective temperature rise is evaluated by supposing that 2/3 of the joule heat goes into a layer of thickness a,

$$Sa\, \delta E_V = 2/3 W_j\, \delta t,$$

$$\delta E_V = C_v\, \delta T,$$

where E_v is the energy density/unit volume,

C_v is the heat capacity/unit volume,

T is the temperature.

For a >d the deposition is taken as being uniform over the conductor thickness d,

$$Sd\delta E_v = W_j \delta t.$$

In general, the exponential factor α is time dependent. Local values defined by

$$\alpha(t) = \frac{1}{H}\frac{\partial H}{\partial t}$$

are used in the computations.

2.2.2 Asymptotic analytic method

This approach is based on the work of reference (4). For semi-infinite conductors, analytic solutions of the non-linear diffusion equation

$$\mu_o \partial H/\partial t = \frac{\partial}{\partial x}(\rho \partial H/\partial x) \qquad \ldots.(3)$$

can be derived for the case of very low and very high fields for particular time profiles of the surface field. The solutions are only valid near the conductor surface; however, this is sufficient to satisfy the requirements of equation (1). Further, the solutions are only valid for materials with properties

$$C_V \text{ independent of } E_v,$$
$$\rho = \rho_o(1 + kE_v). \qquad \ldots.(4)$$

These relations are reasonably consistent with real material properties.

For a profile of form $H_s = H_o \exp(\alpha t)$, we have:-

(1) $H \ll H_c$,

$$H(x,t) = H_s \exp(-x/a), \quad \frac{\partial H(x,t)}{\partial x}\Big|_o = -\frac{H_s}{a}, \qquad \ldots.(5)$$

$$E_v(o,t) = \frac{\mu_o}{2} H_s^2. \qquad \ldots.(6)$$

(2) $H \gg H_c$,

$$H(x,t) = H_s\left(1 - \frac{H_c}{H_s}\frac{x}{a} - \frac{1}{4}\frac{H_c^2}{H_s^2}\frac{x^2}{a^2}\right), \quad \frac{\partial H}{\partial x}(x,t)\Big|_o = -\frac{H_c}{a}, \qquad \ldots.(7)$$

$$E_v(o,t) = \frac{\mu_o}{3} H_s^2. \qquad \ldots.(8)$$

H_c is the critical field defined as $(\frac{2}{k\mu_o})^{\frac{1}{2}}$,

E_v is zero for $H = 0$,

$$a = \left(\frac{\rho_o}{\mu_o \alpha}\right)^{\frac{1}{2}}.$$

Substitution of equations (4), (5) and (6) or (4), (7) and (8) into (1) gives:-

$$H \ll H_c, \; R_a = \rho_o(1 + H_s^2/H_c^2)Sn^2/a = \rho_o f_1 Sn^2/a.$$

$$H \gg H_c, \; R_a = \rho_o(H_c/H_s + \tfrac{2}{3} H_s/H_c)Sn^2/a = \rho_o f_2 Sn^2/a.$$

The functions f_1 and f_2 are shown in figure 3. This analysis does not give values of R_s for intermediate fields. However, figure 3 indicates that a sensible extrapolation may be made.

2.2.3 Finite difference method

General solutions of the non-linear field diffusion equation (3) and the heat equation

$$\partial E_v/\partial t = \rho j^2 = \rho(\partial H/\partial x)^2,$$

$$\partial E_v/\partial T = C_v,$$

$$j = \text{current density},$$

can be obtained for any surface profile $H_s(t)$ and any $\rho(T)$, $C_v(T)$. The appropriate finite difference equations are:-

$$H_m^+ = H_m + \frac{\delta t}{4\mu_o(\delta x)^2}(\rho_{m+1} - \rho_{m-1})(H_{m+1} - H_{m-1}) + \frac{\rho_m \delta t}{\mu_o(\delta x)^2}(H_{m+1} - 2H_m + H_{m-1}),$$

$$E_{vm}^+ = E_{vm} + \frac{\rho_m \delta t}{4(\delta x)^2}(H_{m+1} - H_{m-1})^2.$$

The conductor is divided up into a number of equal increments $\delta x(n)$ where the dependent variables have values H_m, E_{vm}, ρ_m at time t

$$x = m\delta x, \qquad d = n\delta x,$$

$$m = 0, 1, 2 \ldots\ldots n.$$

The superscript + denotes values at $t + \delta t$.

A reasonable approximation to the real situation is represented by the boundary condition

$$H_n = 0.$$

2.3 Coil effective resistance

The coil presents a far more complicated surface problem than the armature. Let us consider the two separate components making up the coil effective resistance.

$$R_c = R_J + R_M,$$

where R_J is the component representing joule heating,

R_M is the component representing magnetic energy storage.

The calculation of R_J for the case of steady ac has been the subject of a number of studies. The most general case for the linear problem has been considered in reference (5) which gives the relation

$$R_J/R_S = \nu + \eta^2\chi(\beta u_1 + \gamma u_2),$$

where R_S is the ac resistance of the coil wire when straight, ie, when subjected to skin effects alone.

ν, η, χ, β, γ, u_1 and u_2 are functions of the coil dimensions, the conductivity and the frequency f and account for proximity effects.

In general, one can equate the resistance of a circuit carrying an exponential current profile to an ac resistance of that circuit,

$$R_J(\alpha) = R_J(f = \alpha/\pi).$$

In order to estimate temperature rises and hence their effect on R_J the approximation is made that the current flow is uniform in an area of cross-section S_c such that

$$\frac{S_c}{\pi r_w^2} = \frac{R_{dc}}{R_J},$$

where r_w is the wire radius,

R_{dc} is the dc resistance of the coil.

Hence, the energy balance relation is

$$R_J I^2 \delta t = S_c \ell \delta E_v,$$

where ℓ is the coil wire length.

Two approximations are used to estimate R_M:-

(a) It is well known that for large magnetic fields and large rates of field change the joule and magnetic energy densities within a conductor are approximately equal. Hence,

$$R_M \sim R_J.$$

(b) The coil is approximated by a conducting layer of thickness $2r_w$. For such a layer with the boundary condition of H = 0 at the outer surface, the results of section 2.2.1 may be applied,

$$R_M = R_a - \frac{1}{2} R_e k',$$

$$= \frac{\rho n^2 S}{2a} \left((2A - 1) + 4A(1 - A) 2r_w/a \right),$$

$$S = 2\pi r_c \ell_o,$$

where r_c is the coil radius,

ℓ_o is the coil length.

3. BASIC INPUTS TO THE MODEL

The electrical equivalent circuit model of section 2 will require input information over and above the static dimensional description of the generator.

3.1 Conductor properties

The conductor property of paramount interest is the electrical resistivity. Because a wide range of temperatures may be encountered, the data

must cover many thermodynamic states, ie, solid, liquid, vapour, plasma. The resistivity variation employed with the current model is shown in figure 4 where the two conductors Cu and Al are taken as examples.

Reference (6) provides data in the solid region and for a limited range in the molten region. The molten data are linearly extrapolated to the boiling point. A further linear approximation is taken from the boiling point to a temperature of $2 \times 10^{4\,o}K$, where the plasma resistivity model of reference (7) is employed. Reference (8) effectively gives the plasma conductivity as

$$\frac{1}{\rho} = \underbrace{\frac{8.35\Sigma_o^2 h^3 n_e}{m_e^2 e^2 Z}}_{\substack{\text{(degenerate)} \\ \text{(plasma term)}}} + \underbrace{\frac{8\pi\Sigma_o^2}{(2m_e)^{\frac{1}{2}} Ze^2}(kT)^{3/2}}_{\substack{\text{(classical)} \\ \text{(plasma term)}}},$$

which, on inserting values for physical constants, reduces to (Z = 1),

$$\frac{1}{\rho} = \frac{n_e}{1.12 \times 10^{23}} + 2.92 \times 10^{-3}\ T^{3/2}\ (\Omega m),$$

where n_e is the free electron density (m^{-3}).

Further,

$$E_V = \frac{3}{2} n_{n+i} kT,$$

where n_{n+i} is the density of neutrals + ions and k is the Boltzmann's constant.

Figure 4 is based on the approximation of one free electron per atom.

Magneto-resistance effects are expected to be small.

Piezo-resistance effects arising through magnetic forces exerted on the conductors are expected to take the Bridgman form

$$\frac{\rho_v}{\rho_{vo}} = \left(\frac{v}{v_o}\right)^y,$$

where v and v_o are the specific volumes at the test and zero pressures respectively. Exponent values for Cu and Al are 2.7 and 3.3 respectively.

Table 1 shows the enthalpy relations up to the boiling point for Cu and Al.

TABLE 1

Parameter	Cu Value	Al Value
$C_{VS}(0)$	3.4 MJ m^{-3} deg^{-1}	2.4 MJ m^{-3} deg^{-1}
s_{VS}	2.36×10^{-4} deg^{-1}	5.0×10^{-4} deg^{-1}
$C_{VL}(MP)$	4.07 MJ m^{-3} deg^{-1}	2.55 MJ m^{-3} deg^{-1}
s_{VL}	0.0	0.0
L_F	1.6 GJ/m^3	1.08 GJ/m^3
L_V	48 GJ/m^3	30.5 GJ/m^3

where the specific heat/unit volume relations have the form

$C_{VS} = C_{VS}(0)(1 + s_{VS}T)$ for the solid conductor,

$C_{VL} = C_{VL}(MP)(1 + s_{VL}(T - T_{MP}))$ for the liquid conductor,

T = ^{o}C,

T_{MP} = melting point,

L_F is the latent heat of fusion,

L_V is the latent heat of vaporisation.

3.2 Armature dynamics

The time dependent geometry will be determined to a large degree by the motion imparted to the armature by its explosive loading. The model

described in this report does not generate this motion but uses it as input. Such information can be generated either through experiment or hydrocode simulation. In the former case, the expansion characteristics are determined in the main from high speed photographic diagnostics. Both framing camera photographs of the armature and streak camera records of suitably arranged flashgaps are used to build up a description of the funnelling action. Such experiments are also important in determining the condition of the conductor during its expansion, ie, how far can it expand before deterioration, such as cracks which can impede current circulation, sets in? Alternatively, the expansion of the shock loaded armature can be determined from hydrocode study. Such an approach will also give information on the shock induced temperatures in the conductors. Both approaches are compatible as far as the expansion characteristics are concerned.

The end result of both approaches is basically the cone expansion angle. In general, the armature expands in the form of a cone with fixed angle whose truncated apex is displaced from the original position of charge initiation by the product of detonation velocity × time from initiation, as indicated in figure 1. Such a characteristic is easily inputted into the model described in this report. In practice this simple description is not completely representative. For instance, expansion characteristics will be perturbed by the effects at the armature ends. However, it is customary to employ armatures which overlap the coil so that such effects are effectively removed. Although the cone angle does vary along the cone at any particular instant in time a mean angle approximation represents a good compromise.

The explosively induced expansion of the armature represents the only noticeable contribution to motion when magnetic field strengths are reasonably small. However, as fields increase electromagnetic forces become sufficiently intense so as to perturb the motion of the armature and to induce movement in the coil. Such forces play an increasingly important role as the generator is scaled up in size. The model adopts the following approach.

Magnetic fields are assumed to be parallel to the conductor surfaces and produce forces normal to those surfaces. The coil is given a field induced expansion velocity and the armature's explosively induced velocity has a field induced reduction. Coil distortion along its axis is not considered. Because the surface magnetic pressure

$$p_m = \frac{1}{2}\mu_o H_S^2 = \frac{1}{2}\mu_o n^2 I^2$$

rises very rapidly during the period where it is significant, then a Hugoniot approximation can be used to relate particle velocity to the magnetic pressure

$$p_m = \rho_o D_S u,$$

where ρ_o is the density at zero pressure,

D_S is the shock velocity,

u is the particle velocity.

Most metals have a linear relation of the form

$$D_S = D_o + mu,$$

where D_o and m are constants.

The simple linear Hugoniot relations for Cu and Al have the coefficients shown in table 2.

TABLE 2

	D_o, m/s	m	ρ_o, kg/m^3
Cu	4000	1.5	8900
Al	5200	1.4	2800

4. CODE RESULTS

The generator output will depend on a large number of parameters. Code studies will, in general, be directed towards identifying the important parameters and deriving optimum values. In this section some typical examples of output are given, together with some selected parameter trends. A selected comparison with experimental data is also presented.

A generator having the following parameter description is taken as the basis for the examples:-

Length: 31.8 mm

Armature (Cu): radius 7.95 mm; thickness 0.5 mm; expansion half-angle 14^{o}

Coil (Cu): radius 15.2 mm; wire diameter 0.376 mm (28 SWG); pitch 0.442 mm

Explosive detonation velocity: 8800 m/s

Load: $R_{\ell} = 50\ m\Omega$, $L_{\ell} = 13\ nH$

Room temperature: $20^{o}C$; Shock release temperature of armature $170^{o}C$

Priming current: 200 A

Unless otherwise stated, the following examples are directly relevant to the above generator.

4.1 Typical results

Some of the typical code outputs are shown in figures 5 to 15. In this example, the generator is overdriven with a high priming current of 2500 A in

order to exaggerate some of the thermal effects. In each figure a family of up to 15 curves are shown, each one representing a different winding pitch value. The time in each figure is referenced to armature first movement at the beginning of the coil (it is assumed that the generator is short-circuited from the priming supply at this stage).

Figure 5 shows the number of turns left in the coil. First crowbar of the armature on the coil is indicated by the onset of the decrease in the number of turns. At 6.2 μs the generator has been completely short-circuited.

Figure 6 shows the corresponding generator inductance as defined in section 2.1.

Figures 7 and 8 show the mean effective armature and coil temperatures as defined by the models in sections 2.2.1 (equivalent skin depth) and 2.3. The profiles for the armature in this example have a temperature level of 170°C which is derived from the shock heating of the conductors from a room temperature of 20°C. Until ~ 3 μs there will be regions of shocked and unshocked armature; thereafter all the armature will have been shocked. The profile in figure 7 will represent the hottest section of the armature. For this example the current and hence the heating will peak in the region 5.5 to 6 μs so that the steep profiles turn over and show a plateau at this point. Although the curves extend to about 7 μs, they have no significance after 6.2 μs because the generator is completely short-circuited at this time. Curves 1, 2, 3 and 4 are different in that 1, 2 and 3 pass through the melting transition of Cu at 1083°C and continue into the molten region, and 4 reaches the transition but does not emerge from it. The remaining curves are all contained within the solid regime. Figure 9 shows the latent heat curve that complements figure 7. Curves 1, 2 and 3 acquire the latent heat of fusion for Cu (1.6 GJ/m^3) before heating terminates, whereas curve 4 only acquires 0.5 GJ/m^3 before heating ceases. Figure 8 for the coil is similar to figure 7 apart from the room temperature (20°C) starting value, and the higher temperatures reached. Figure 8 and its latent heat complement figure 10 indicates that curves 1 to 12 pass through the melting transition and curve 13 accumulates ~ 0.5 GJ/m^3 of latent heat before heating stops.

For the alternative armature models described in sections 2.2.2 and 2.2.3 the armature thermal condition will be described by thermal energy density curves for the surface.

Figure 11 shows the armature effective resistance as defined by section 2.2.1. It increases up to first crowbar time through the increasing shocked area of the armature and the increasing exponential factor associated with the current increase. After first crowbar, the resistance decreases due to the reduction in armature area. However, because of the extreme joule heating, curves 1, 2 and 3 show terminal resistance spikes.

Figure 12 shows the joule component of the coil resistance R_J (in this example the approximation $R_J \sim R_M$ has been used). The profiles are similar to armature resistance, however, in this case the increase up until first crowbar time is due entirely to the increase in the current exponential factor. The more severe heating in the coil causes most of the curves to exhibit the terminal resistance spike

The armature's magnetically-induced particle velocity is shown in figure 13. Because the coil and armature conductors are both Cu in this example both will exhibit identical profiles. The armature's magnetically-induced velocity will be in the opposite sense to the explosively-induced particle velocity and hence will, in addition to the coil expansion velocity, increase the time required to completely short-circuit the generator. This point is amplified in figure 5 where it is seen that the curves reach zero at slightly differing times. The highest particle velocity in figure 13 for curve 1 represents only 6% of the explosively-induced velocity. In general, appreciable slowing down of device operation only occurs for generators which are significantly larger than the example under consideration. Small generators are unable to transduce large fractions of armature kinetic energy into magnetic energy because of the large joule losses incurred at the high temperatures produced.

Figure 14 shows the generator's current gain as a function of time. The values are somewhat on the low side because the generator is overdriven with the 2500 A priming current. The time of peak varies, ie, the larger the gain

the sooner severe heating sets in resulting in a turn-over. Optimum output is obtained in this example for a wire diameter:pitch ratio of 0:6 (although the optimum is not sharp). In general, this optimum occurs for close-wound coils but it does tend to wander from this position slightly when conductors get hot. It will also be noted that current peak occurs before the generator is completely short-circuited. Although joule heating is a significant factor in producing this effect in this example, it is a general result even for cold conductors. Near the end of generator operation the dI/dt driving function (slope of figure 6) is no longer capable of offsetting the circuit resistance in the relation

$$\frac{dI}{dt} = \frac{-I(\frac{dL}{dt} + R)}{L}.$$

Finally, figure 15 shows the typical increase with time of the current exponential factor $\alpha(t)$. In this model the factor retains its peak value after peak current.

4.2 Compatibility of models

In section 2 a number of alternative models for computing circuit parameters were given. In general, the alternative approaches are quite compatible. The alternative approaches for calculating generator inductance are consistent to within ~1%. The first of the two models for calculating R_J in section 2.3 gives a slightly higher result. However, unless the load impedances are small, the current amplifications are not too dissimilar.

An illustration of the degree of agreement among the three models for computing armature effective resistance is shown in figure 16 for the example generator already described. The peak current amplifications are shown as a function of priming current for a wire diameter/winding pitch = 0.8. Figure 16 indicates that the equivalent skin depth and finite difference models are virtually equivalent. Further, the asymptotic approach is consistent with the other two models at the extremes of the range but shows a divergence of up to 5% in the intermediate region. This result is not unexpected and indeed the divergence can be reduced by using a more elaborate extrapolation approach for the asymptotic model. The asymptotic approach is only correct in principle for

$H_c \gg H \gg H_c$. In figure 16 the priming current which leads to H_c at peak amplification is shown. The peak current amplification is most strongly influenced by the armature resistance near peak time where the circuit's time constant is small. Hence, the asymptotic approach is only expected to be correct for priming currents significantly above and below ~ 200 A for this example. In figure 16 a linear extrapolation for the armature resistance was taken for the intermediate region.

$$f = f_1\left(\frac{H_c}{\varepsilon}\right) + \left[\frac{H - \frac{H_c}{\varepsilon}}{\varepsilon H_c - \frac{H_c}{\varepsilon}}\right]\{f_2(\varepsilon H_c) - f_1(H_c/\varepsilon)\},$$

with $\varepsilon = 2.5$. However, the result is not very sensitive to the value assigned to ε. Although a better, more elaborate extrapolation is possible, the simple linear approach is deemed to be satisfactory.

The more exact finite difference approach is regarded as the standard. However, because it requires significantly more computer time it is used as a check, whereas the other models are employed for large-scale parameter variation studies.

4.3 Load effects

The example generator's performance, as a function of load resistance and inductance, is shown in figure 17. The influence of load changes is only highly significant for low load values. The predictions are compared with experimental data for this generator (9). Agreement is seen to be good over a wide range of load values both in absolute value and trend.

4.4 Influence of wire diameter and winding pitch

The generator's performance is maximised for an optimum combination of wire diameter and winding pitch. The optimising conditions for current and energy gains are in general different. This effect is illustrated for our

example generator in figure 18. Maximum current gain implies maximum rate of current rise. On the other hand maximum energy gain ensures the highest output current for a given system size (and priming energy).

Figure 18 shows that for each wire diameter there are optimum pitch conditions for current and energy gain. The former lie in the vicinity of close-wound coils while the latter occur at larger pitches. Further, the optimised wire diameter is larger for energy gains. The optimising conditions depend on the system parameters. For instance, as priming currents, with associated heating, are increased optimum conditions tend towards larger wire diameters and pitches. This effect has already been noted in figure 14 and section 4.1.

The example shown in figure 18 indicates that the conditions for optimum current and energy gains are significantly different. However, a compromise choice can be made which gives good performance in both aspects.

4.5 Influence of expansion angle and expansion ratio

The expansion ratio is defined as coil radius/armature radius. In figure 19 the expansion ratio is varied through changes in armature diameter alone, ie, fixed overall generator size. The most striking result is that output improves significantly with expansion angle. This is attributable to the reduction of generator run time. However, the characteristics show far smaller effects for variation of expansion ratio at fixed expansion angle. In fact, the energy gains show something of an independence of expansion ratio. This result is not unexpected because the most significant transduction of energy and loss through diffusion occurs during the latter stages of the generator's operation. During these final stages, the generator's geometry will be independent of the initial expansion ratio. Because in practice one has to maintain the physical integrity of the expanding armature in order to maintain its good current carrying characteristics, a greater expansion ratio will be associated with a thicker heavier conductor and less explosive. This would suggest a reduction of expansion angle and hence some drop in energy gain with increasing expansion ratio. A lower limit for the desirable expansion ratio would be that set by the condition for the armature to reach its terminal expansion velocity. This limit is of the order of 1.5.

A great deal of effort has been expended in the past in order to increase the expansion ratio significantly. The above result suggests that alternatively one should look for minimum conductor thickness at more modest expansion ratios.

4.6 Influence of priming current

The CMF generator described in this report is essentially a current amplifier. At low priming current levels, the current and energy amplifications are independent of priming current. However, at higher levels, joule heating becomes significant leading to a loss of performance. In fact the output shows a limit in total current. However, by this stage the generator/priming assembly is working inefficiently on an output/volume basis and a bigger generator or one with a different coil is required. At the higher current levels, magnetic pressure may also contribute to the loss in amplification. This influence will be small in small generators. Some of these features are illustrated in figure 20. When the total output current for the 28 SWG coil has reached its upper limit, the generator's current amplification has dropped to about a third of its low current value. Figure 20 indicates that for this small generator the magnetic pressure contribution to the loss of amplification is small. Additionally, figure 20 illustrates how optimum wire diameter increases with priming current.

Good agreement is shown between the predictions and experimental data (9).

4.7 Influence of resistivity

One of the material physical properties that has a significant influence on generator output is the conductor resistivity. This applies both to the coil and armature.

Figure 21 shows the generator output as a function of priming current for various ambient temperatures, both above and below normal room temperature. The curves, which show a significant temperature dependence at a low priming level, converge for higher priming currents where the initial temperatures differences are offset by joule heating. However, in practice, changes in

ambient temperature are likely to produce effects in addition to resistivity changes. For instance, explosive performance may change and differential expansions will produce a poorer fit between the armature and its explosive charge, especially at very low temperatures.

Figure 22 shows resistivity effects through the use of different conductor materials in the coil and armature. All four combinations for the two conductors Cu and Al (armature and coil) are taken as examples. The results, for two values of priming current, show the expected significant loss of output as one moves from Cu to Al. However, the results for the Al armatures will be a little improved in practice because, being somewhat lighter, they will have slightly larger expansion angles. The results in figure 22 are all for an expansion angle of 14^{o}.

5. CONCLUSIONS

A model for a compressed magnetic field generator employing a round wire single pitch helical coil has been presented. Magnetic diffusion losses, including joule heating, in botn armature and coil are taken into account, together with the dynamic effects of magnetic pressure.

The aim of the computational side has been to avoid undue mathematical complexity while still incorporating the essential physical features. Although alternative techniques are described for computing circuit parameters, these lead to consistent results. As a general guide, ten complete runs on an IBM 370/168 machine take ~ 1 min. However, the duration may be increased by an order of magnitude when the finite difference model is employed for computing armature effective resistance. This more exact method is usually used only as a "spot check". The modest run time enables one to carry out extensive parametric studies quickly and cheaply with a view to minimising the number of time consuming and costly experiments.

The good agreement between prediction and experimental data is particularly encouraging.

REFERENCES

1. M Jones: "An Equivalent Circuit Model of a Solenoidal Compressed Magnetic Field Generator". Second International Conference on Megagauss Magnetic Field Generation and Related Topics, Washington DC, May-June 1979. To be published

2. F W Grover: "Inductance Calculations Working Formulae and Tables". Dover Publications Inc (1962)

3. F Herlach: J Appl Phys, 39, 5191 (1968)

4. J D Lewin and P F Smith: Rev Sci Instr, 35, 541 (1964)

5. A H M Arnold: Proc IEE, 98, 94 (1951)

6. "Metals Handbook". Edited by Philpott. Product Journals (1968)

7. G Lehner: "Proceedings of the Conference on Megagauss Magnetic Field Generation by Explosives and Related Experiments". Edited by H Knoepfel and F Herlach. Published by European Atomic Energy Community (Euratom), Brussels (1966)

8. H Kneopfel: "Pulsed High Magnetic Fields". North-Holland Publishing Company, Amsterdam-London (1970)

9. J E Gover, Sandia: Private Communication

APPENDIX A

Consider a generator having current I in a coil of n turns/unit length.

The magnetic energy stored in vacuo is

$$W_m = \int_V \frac{\mu_o}{2} (\vec{H}.\vec{H}) dV, \qquad \text{(A1)}$$

where the field is a function of time and position and the integral is take over the volume bounded by the generator conductors.

From the definition of inductance L,

$$W_m = \tfrac{1}{2} L I^2. \qquad \text{(A2)}$$

Differentiation of equations (A1) and (A2) yields

$$\dot{W}_m = \int_V \frac{\mu_o}{2} \frac{\partial}{\partial t} (\vec{H}.\vec{H}) dV + \int_S \frac{\mu_o}{2} (\vec{H}.\vec{H}) \vec{u}.d\vec{S}, \qquad \text{(A3)}$$

$$\dot{W}_m = L I \dot{I} + \tfrac{1}{2} \dot{L} I^2,$$

where $\vec{u}$ is the conductor velocity and S the bounding surface.

Equating terms due to field and volume changes

$$L I \dot{I} = \int_V \frac{\mu o}{2} \frac{\partial}{\partial t} (\vec{H}.\vec{H}) dV,$$

$$\tfrac{1}{2} \dot{L} I^2 = \int_S \frac{\mu_o}{2} (\vec{H}.\vec{H}) \vec{u}.d\vec{S}.$$

The general circuit relation is

$$\frac{d}{dt} (LI) + RI = 0$$

and the energy balance relation

$$-RI^2 = \dot{W}_m + \frac{1}{2} \dot{L} I^2,$$

$$= \dot{W}_m + \int_S \frac{\mu_o}{2} (\vec{H}.\vec{H}) \vec{u}.d\vec{S}. \qquad \text{(A4)}$$

Further, for the vacuum where electrostatic energy storage is negligible and where there is no dissipation we have

$$\int_S (\vec{E} \times \vec{H}).\vec{dS} = - \int_V \frac{\mu_o}{2} \frac{\partial}{\partial t}(\vec{H}.\vec{H})dV. \qquad \text{(A5)}$$

Substitution of equations (A3) and (A5) into (A4) gives

$$- RI^2 = - \int_S (\vec{E} \times \vec{H}).\vec{dS} + \int_S \mu_o(\vec{H}.\vec{H})\vec{u}.\vec{dS}. \qquad \text{(A6)}$$

The appropriate field equations for the moving conductor are (using standard nomenclature)

$$\nabla \times \vec{H} = \vec{j},$$

$$\vec{j} = \vec{E}_{EFF}/\rho,$$

$$\vec{E}_{EFF} = \vec{E} + \vec{u} \times \mu_o\vec{H}.$$

These may be manipulated to give

$$\vec{E} \times \vec{H} = \rho(\nabla \times \vec{H}) \times \vec{H} + \mu_o(\vec{H}.\vec{H})\vec{u} - \mu_o(\vec{H}.\vec{u})\vec{H},$$

which on substitution in equation (A6) yields

$$- RI^2 = - \int_S \rho(\nabla \times \vec{H}) \times \vec{H}.\vec{dS} + \int_S \mu_o(\vec{H}.\vec{u})\vec{H}.\vec{dS}. \qquad \text{(A7)}$$

Hence, the energy lost through the vacuum/conductor interface to be dissipated as joule heat or stored as magnetic energy in the conductor can be evaluated through an equivalent circuit or effective resistance R of the form depicted in equation (A7).

If $\vec{H}$ and $\vec{u}$ or $\vec{H}$ and $\vec{dS}$ are everywhere perpendicular, then the second term in equation (A7) is zero.

Further, for an infinitely long system

$$H_S = nI$$

and in the one-dimensional case with fields parallel to the conductor surfaces

$$R = -\frac{n^2}{H_S^2}\int_S \rho H \frac{\partial H}{\partial x} dS.$$

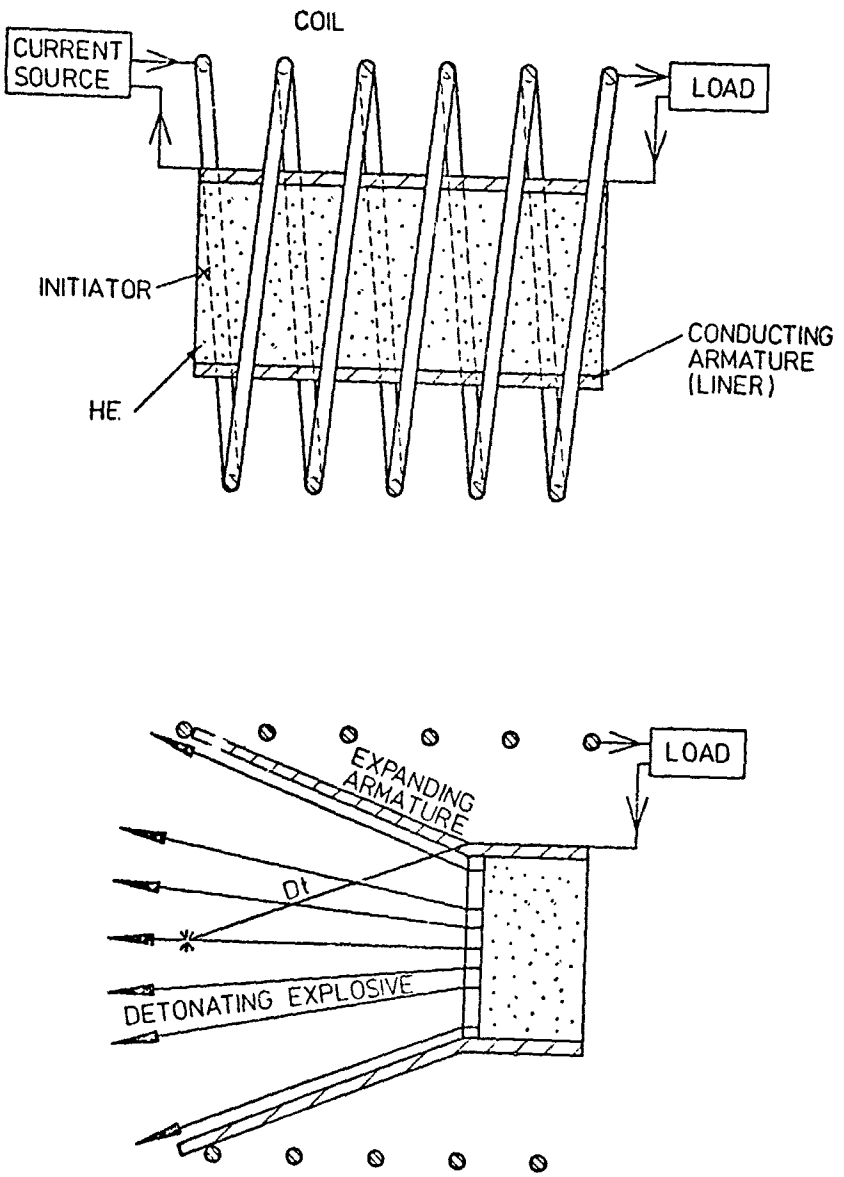

Fig 1
SCHEMATIC OF GENERATOR

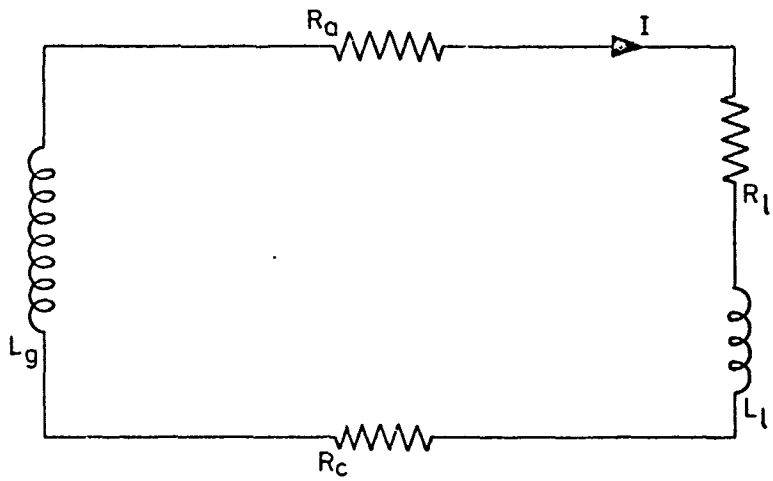

L_g	GENERATOR INDUCTANCE (EXCLUDING LEAKAGE)
L_l	LOAD INDUCTANCE
R_a	ARMATURE EFFECTIVE RESISTANCE
R_c	COIL EFFECTIVE RESISTANCE
R_l	LOAD RESISTANCE
I	CIRCUIT CURRENT

Fig 2

LUMPED EQUIVALENT CIRCUIT
OF GENERATOR

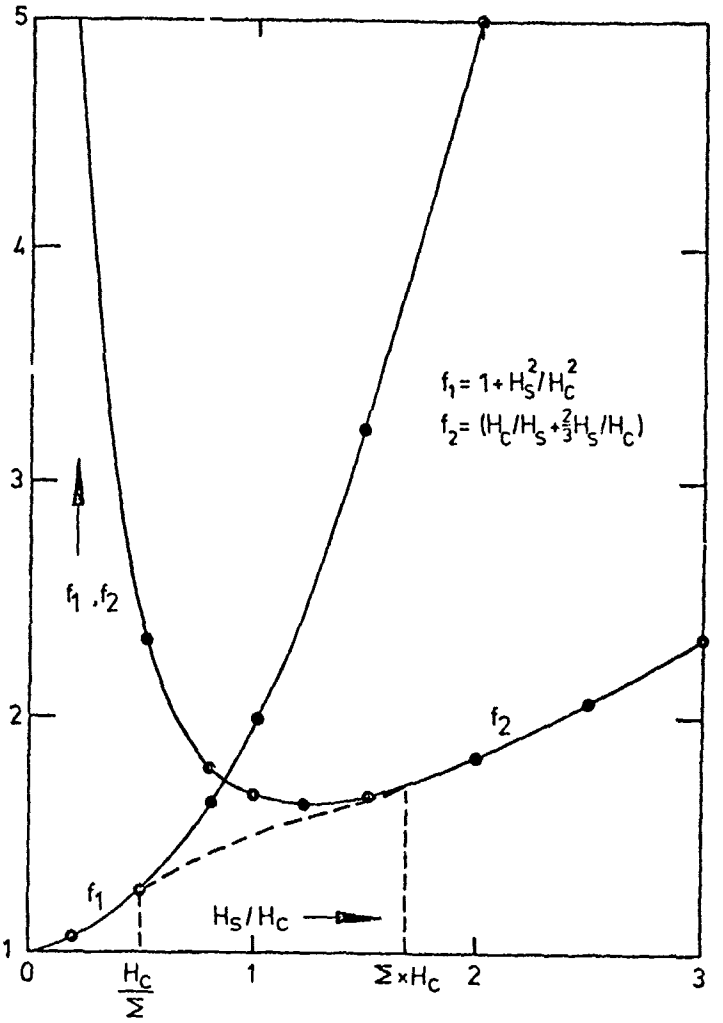

Fig 3

FUNCTIONS f_1 AND f_2 FOR
ASYMPTOTIC ANALYTIC METHOD

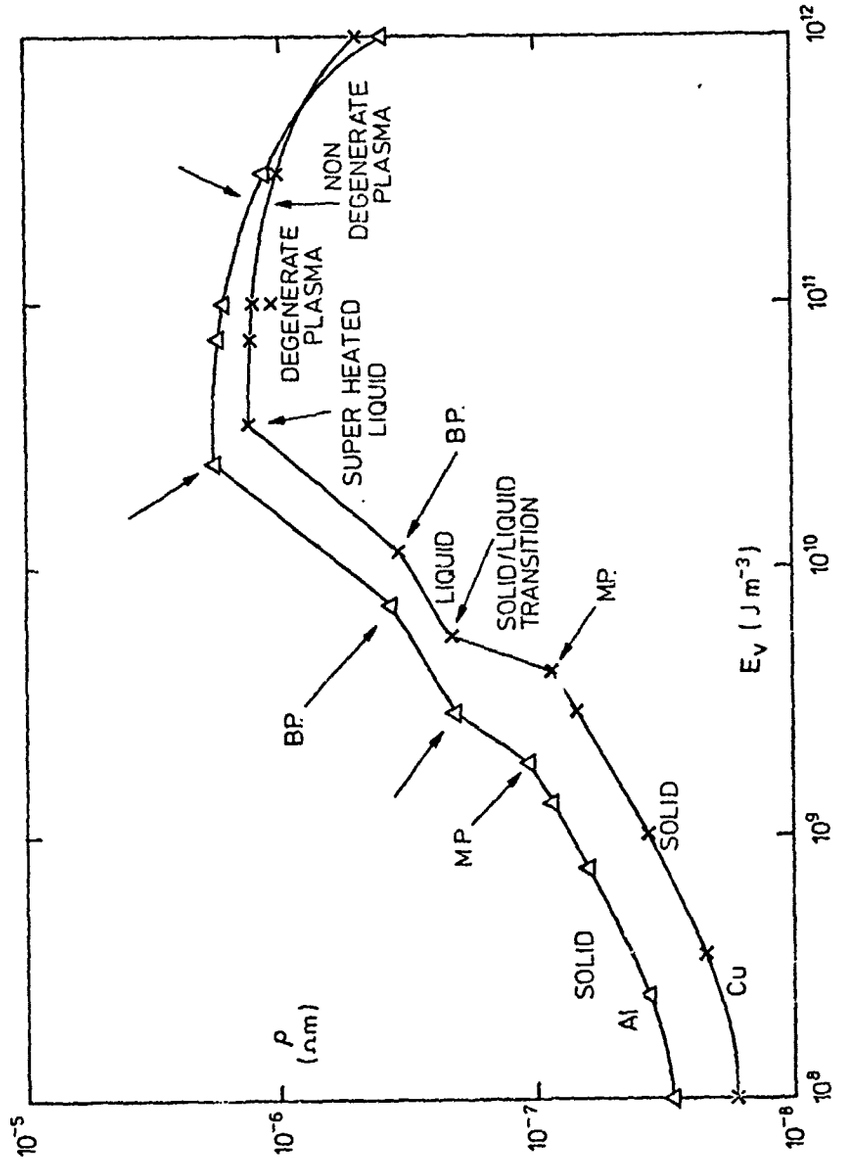

Fig 4

THE HEAT DEPENDENT RESISTIVITIES OF COPPER AND ALUMINIUM

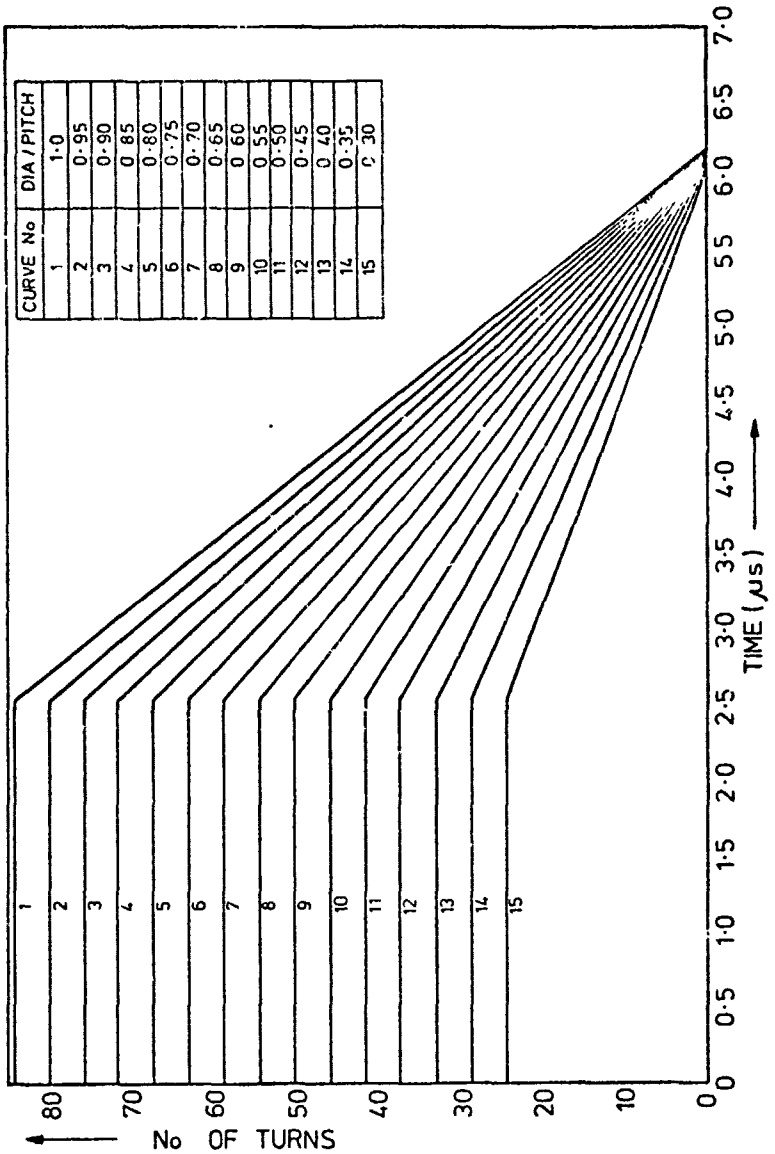

Fig 5
COIL TURNS AS FUNCTION OF TIME

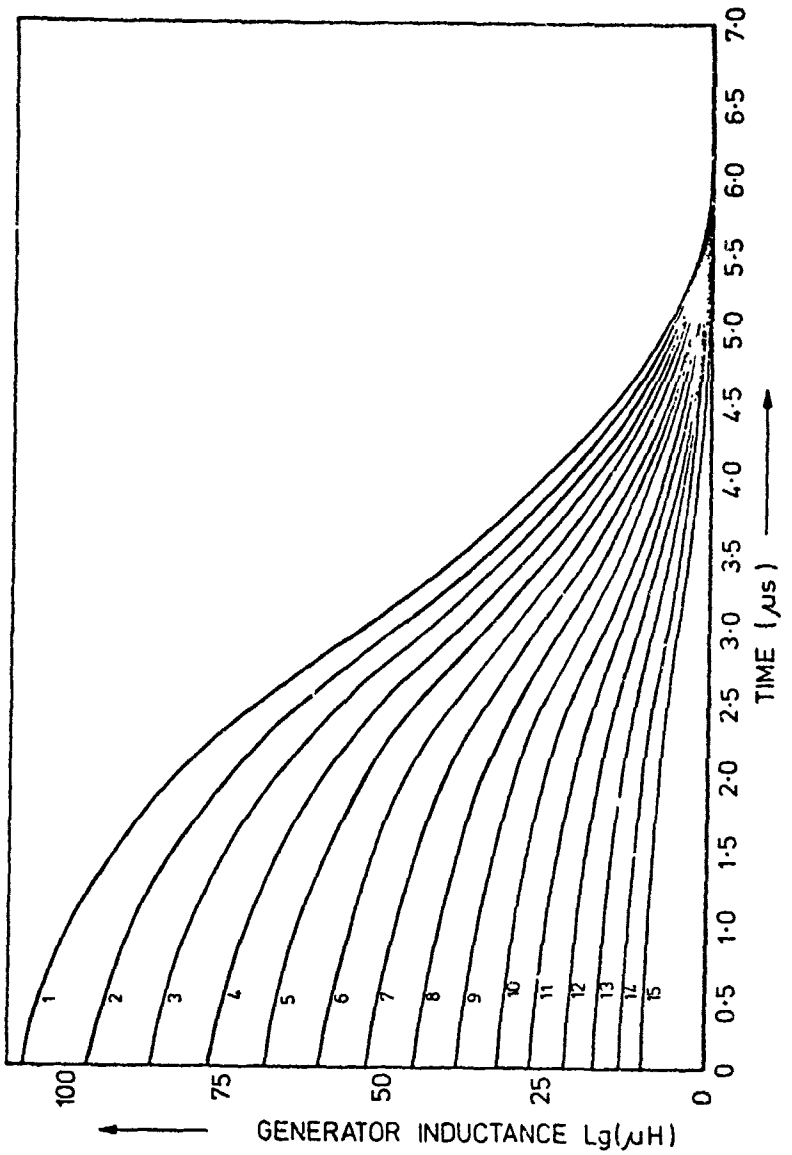

Fig 6

GENERATOR INDUCTANCE
AS A FUNCTION OF TIME

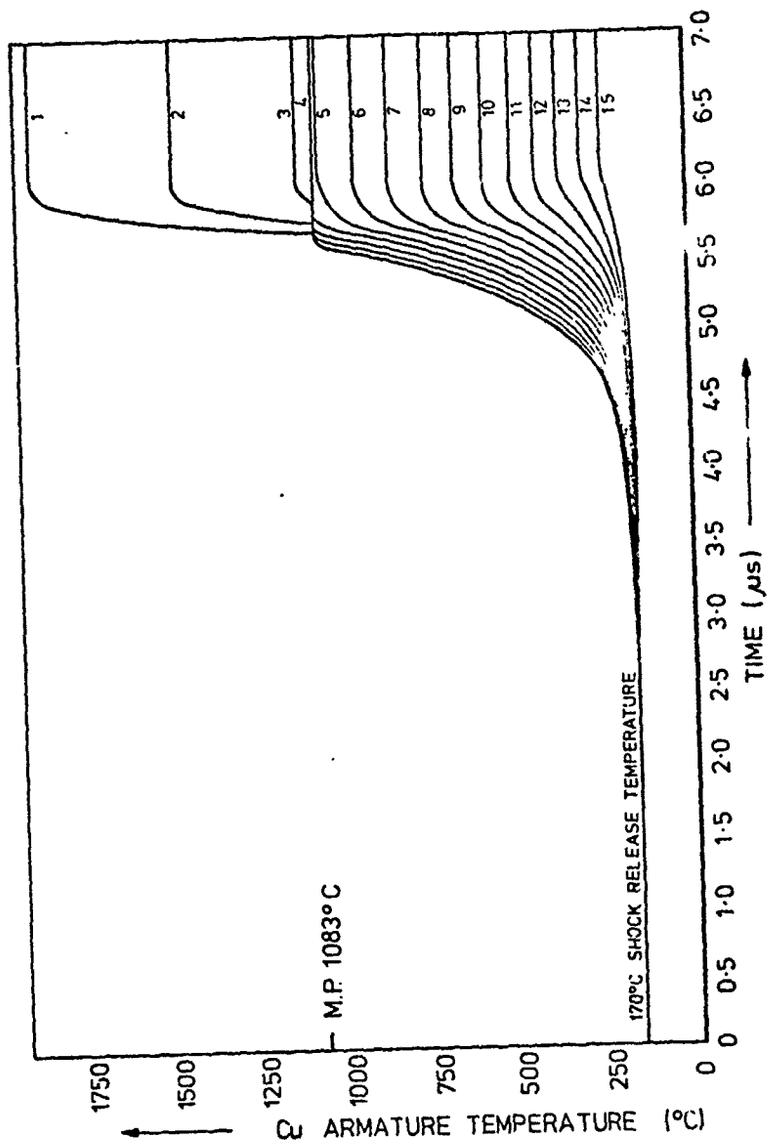

Fig 7

EFFECTIVE ARMATURE TEMPERATURE
AS FUNCTION OF TIME

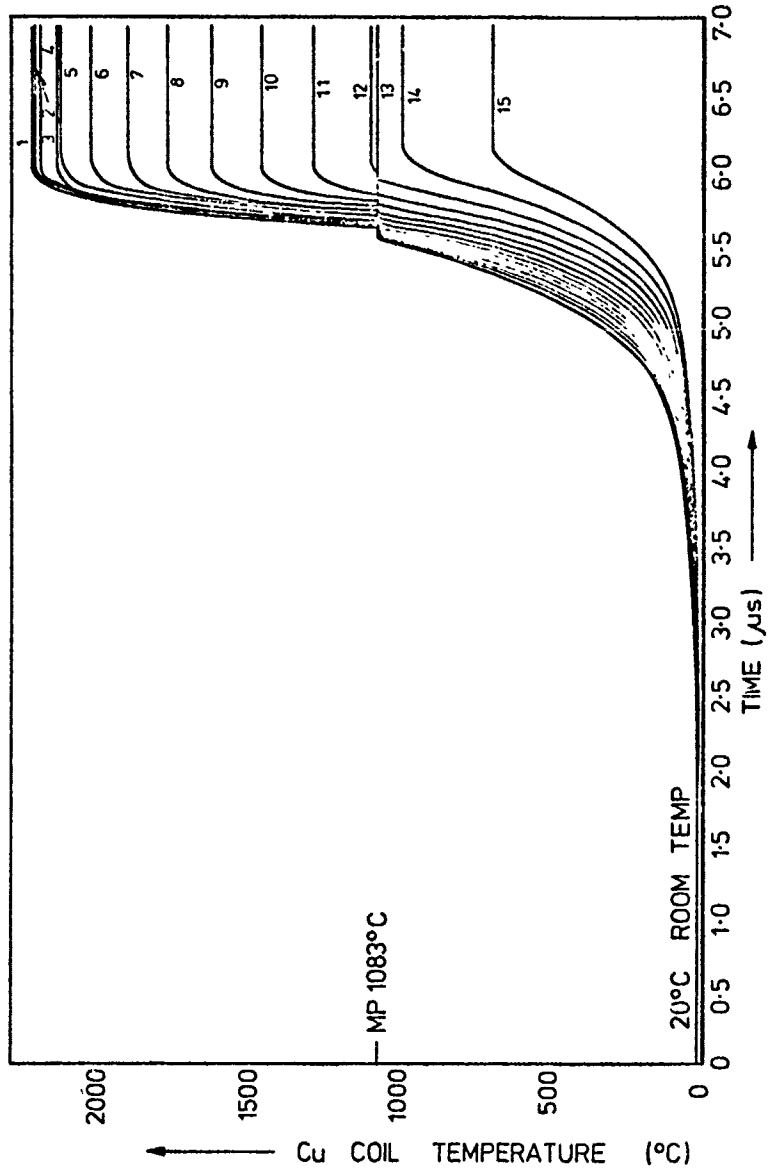

Fig 8

EFFECTIVE COIL TEMPERATURE
AS FUNCTION OF TIME

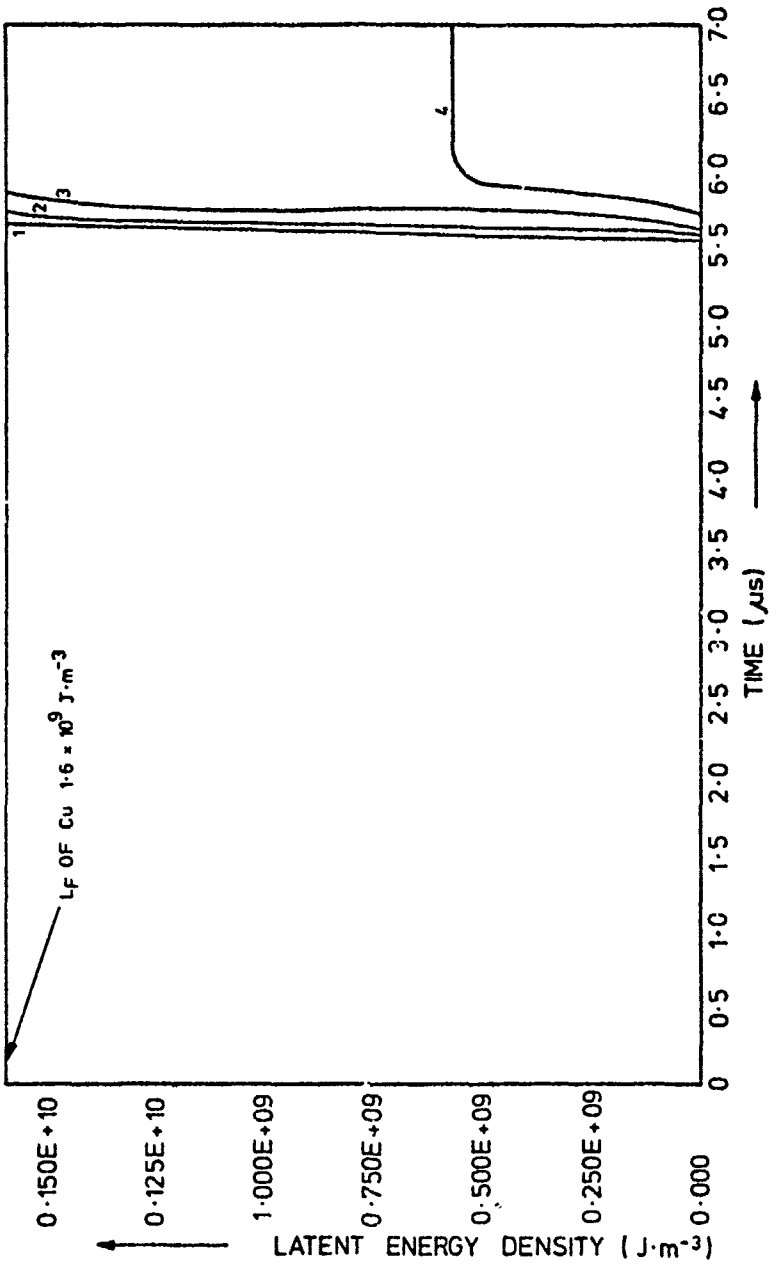

Fig 9

ARMATURE EFFECTIVE LATENT ENERGY DENSITY AS A FUNCTION OF TIME

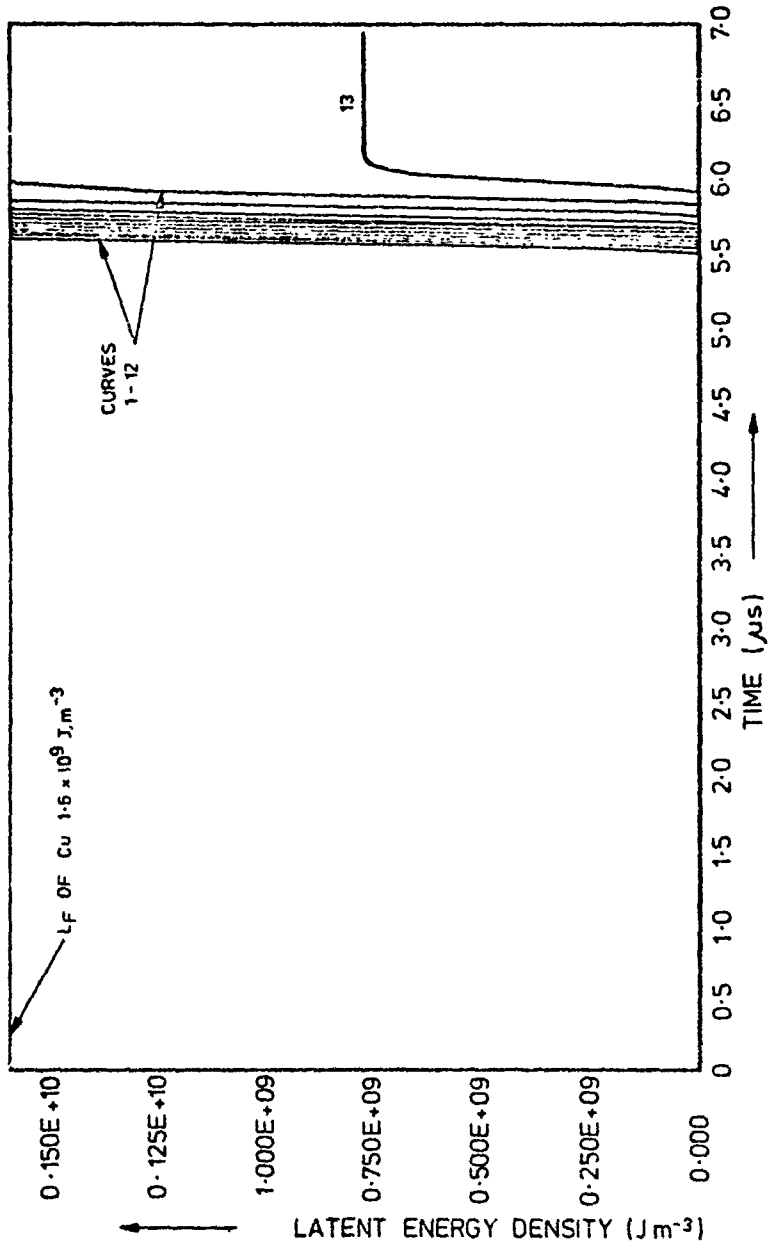

Fig 10

COIL EFFECTIVE LATENT ENERGY DENSITY
AS FUNCTION OF TIME

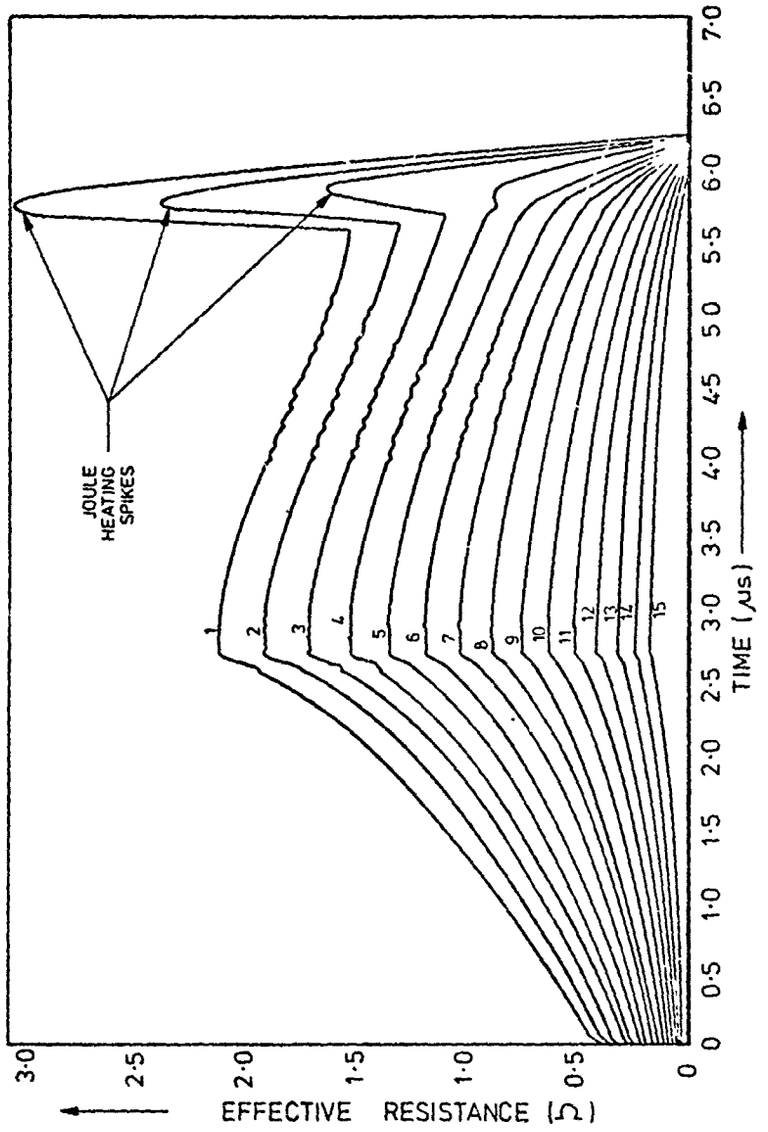

Fig 11

ARMATURE EFFECTIVE RESISTANCE Ra
AS FUNCTION OF TIME

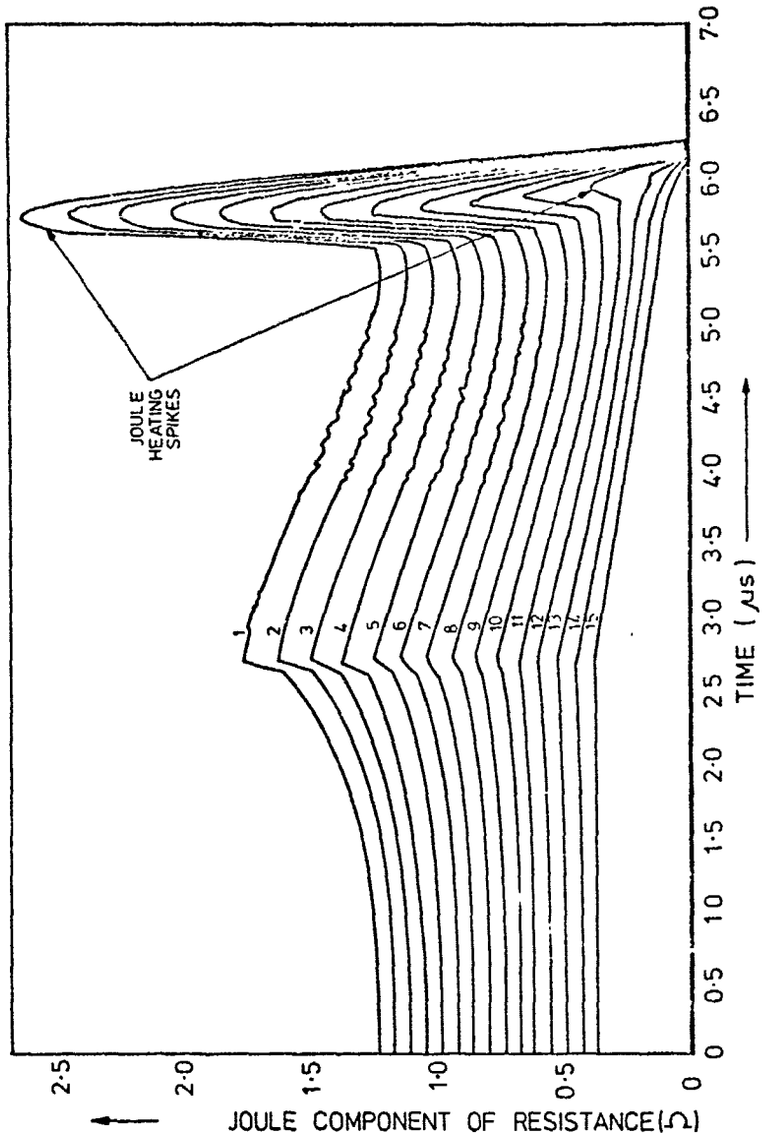

Fig 12

JOULE COMPONENT OF COIL RESISTANCE R_J
AS FUNCTION OF TIME

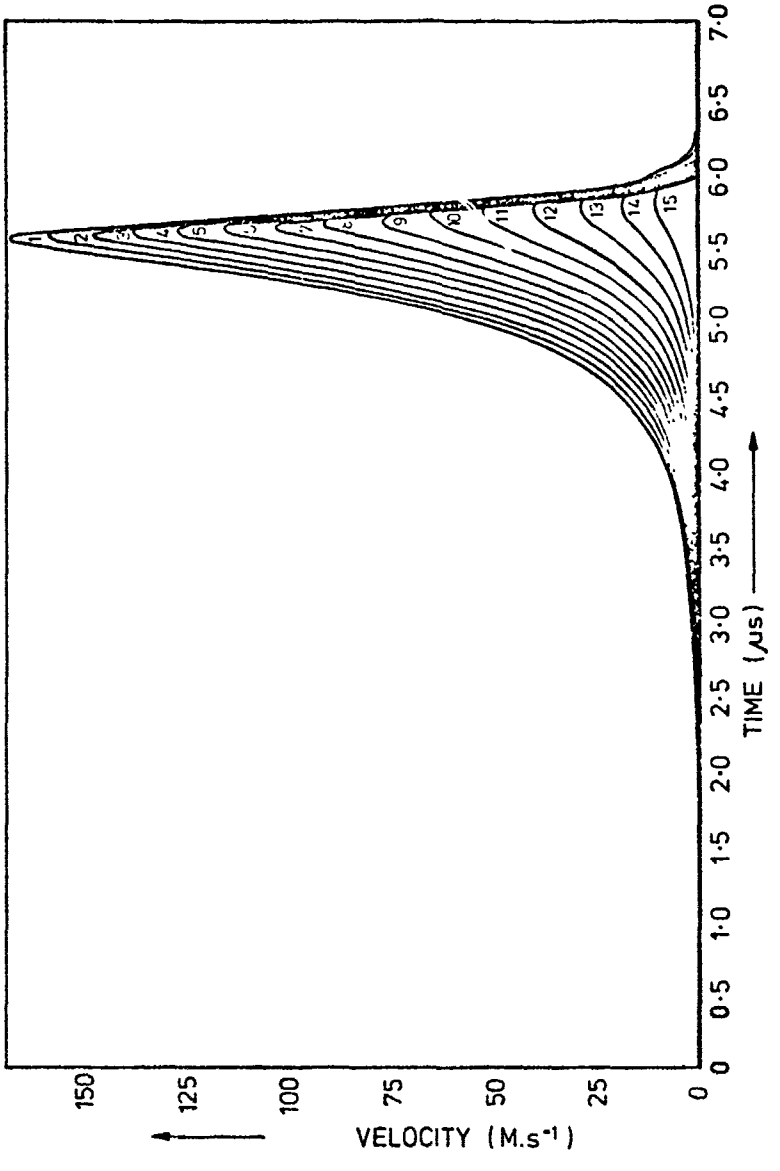

Fig 13

PARTICLE VELOCITY IMPARTED TO ARMATURE BY MAGNETIC PRESSURE AS A FUNCTION OF TIME

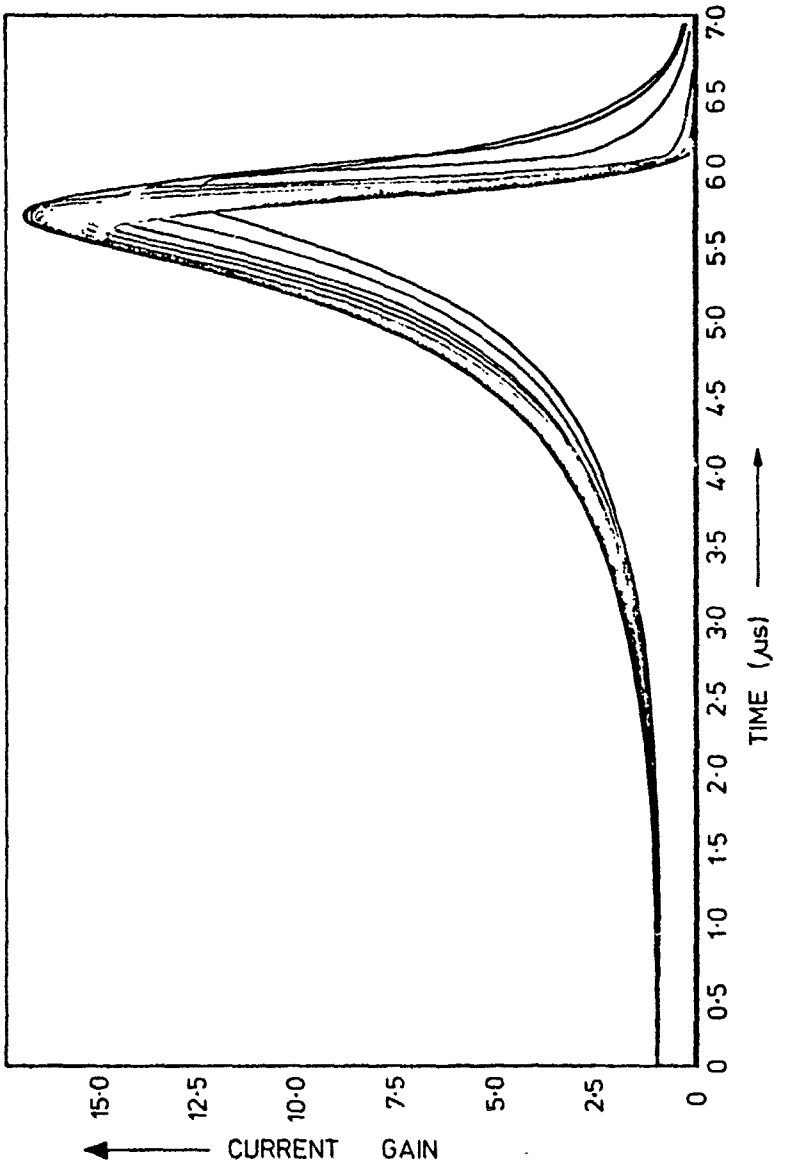

Fig 14

GENERATOR CURRENT AMPLIFICATION
AS FUNCTION OF TIME

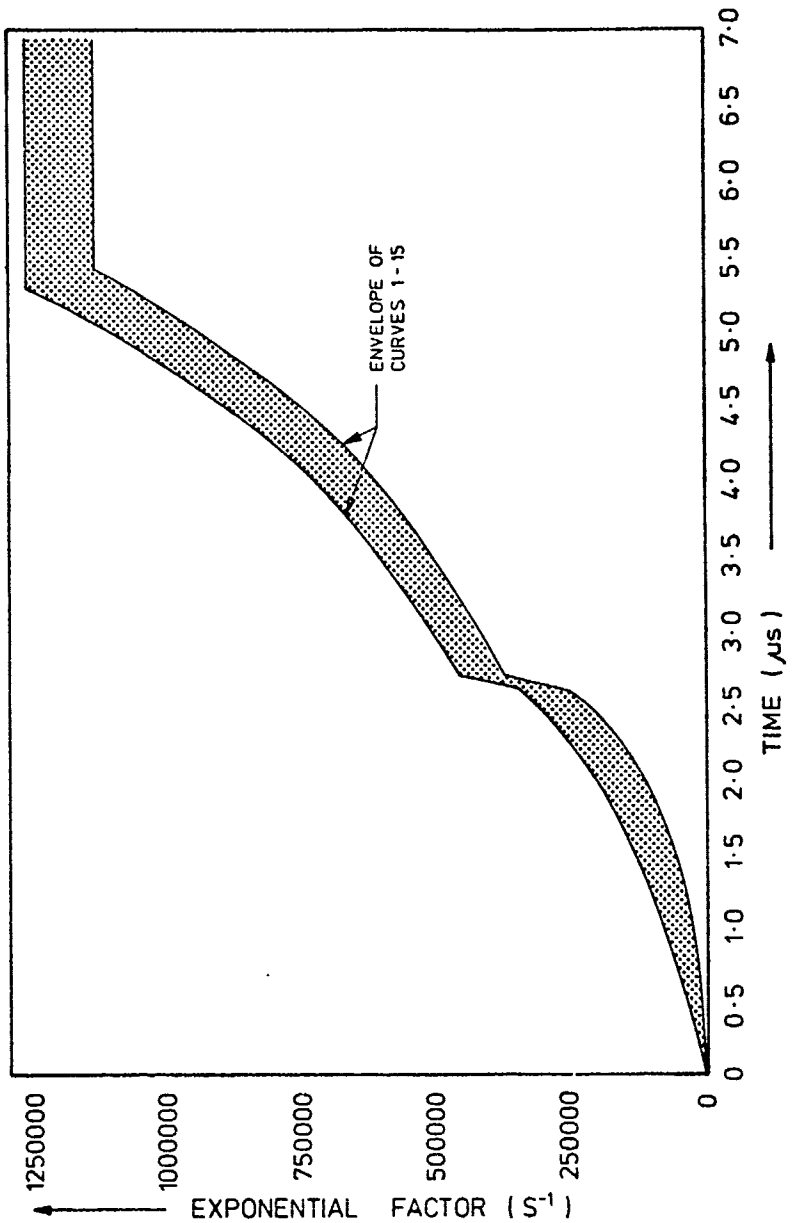

Fig 15

CURRENT EXPONENTIAL FACTOR α
AS FUNCTION OF TIME

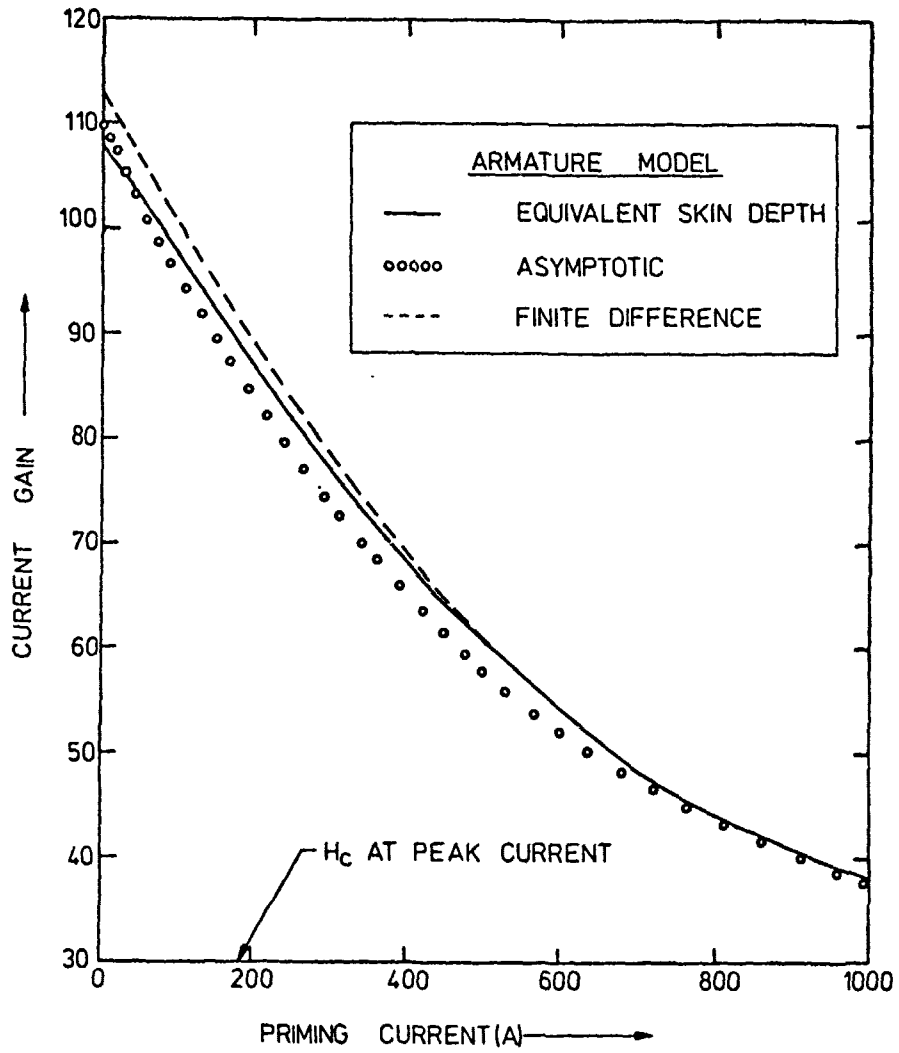

Fig 16

COMPARISON OF ARMATURE MODELS

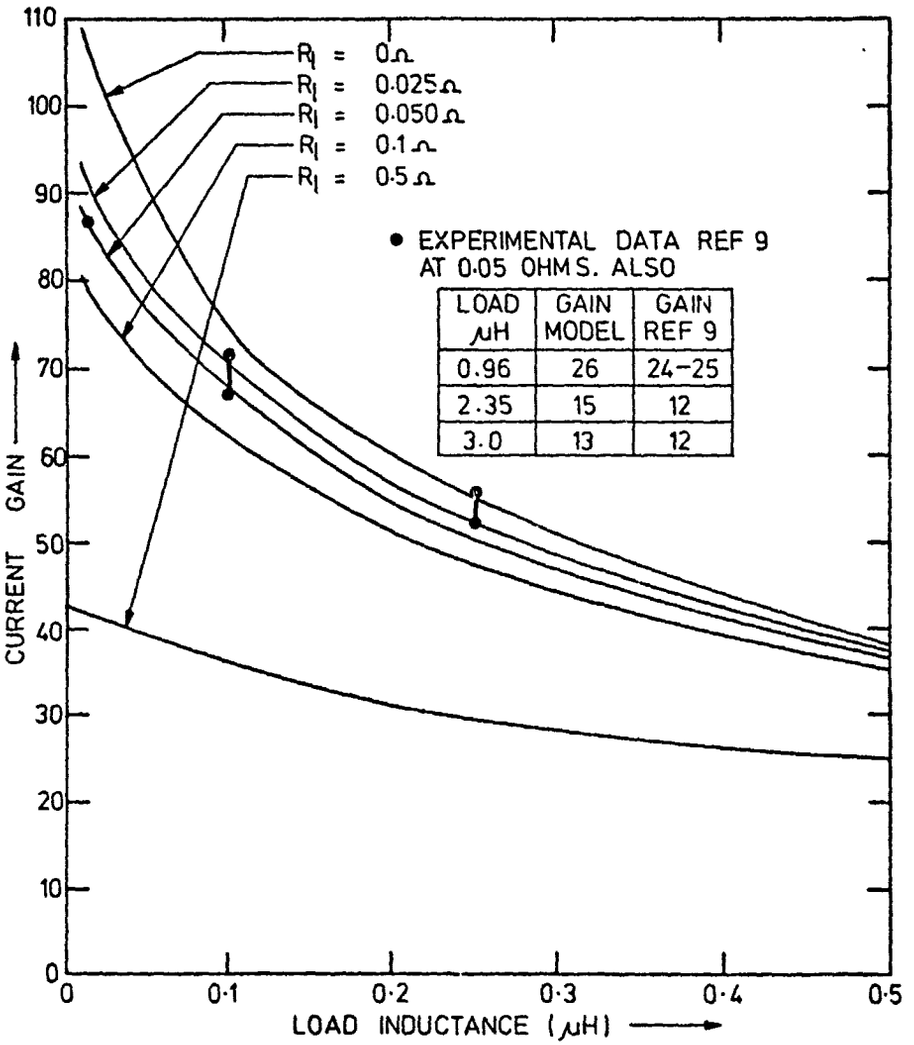

LOAD μH	GAIN MODEL	GAIN REF 9
0.96	26	24–25
2.35	15	12
3.0	13	12

Fig 17

OUTPUT AS A FUNCTION OF LOAD

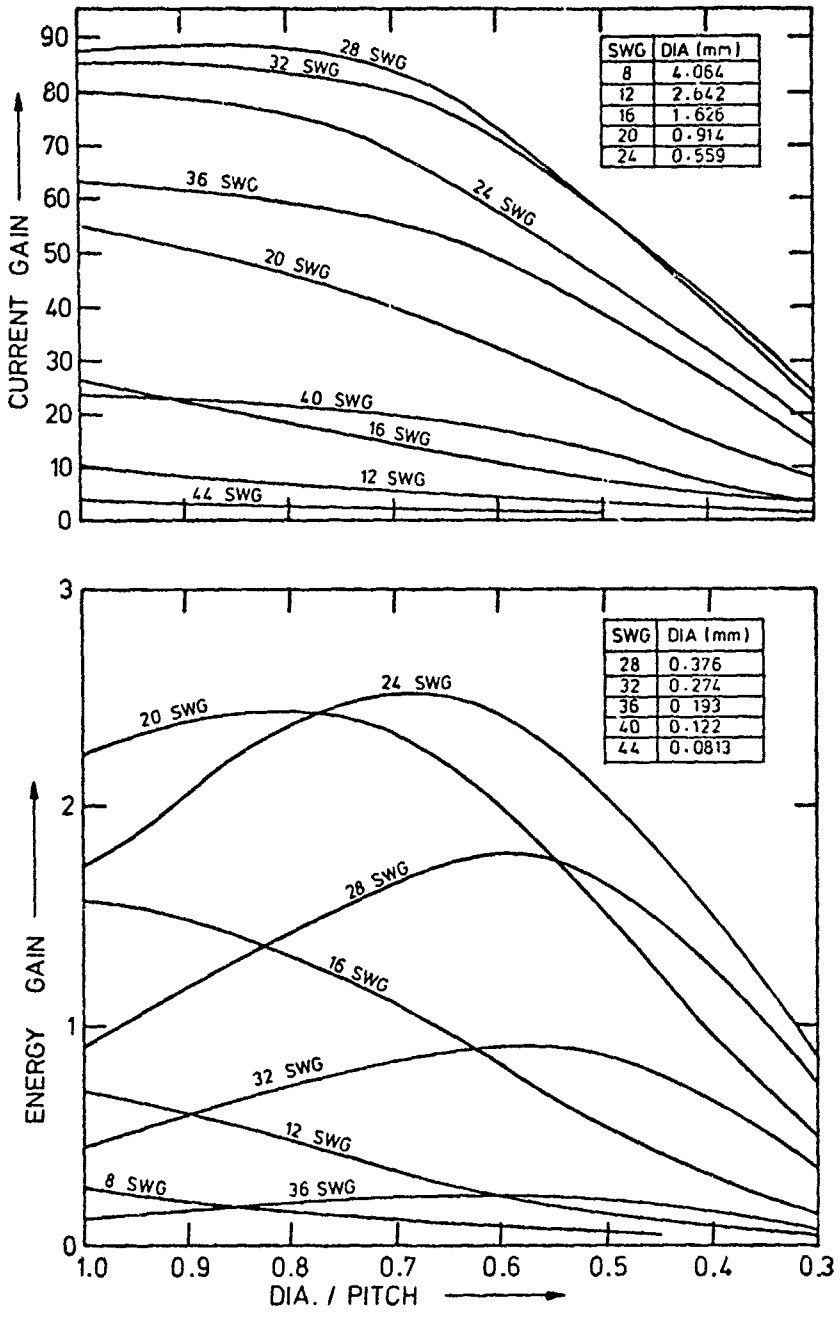

Fig 18

OUTPUT AS A FUNCTION OF WIRE DIAMETER AND PITCH

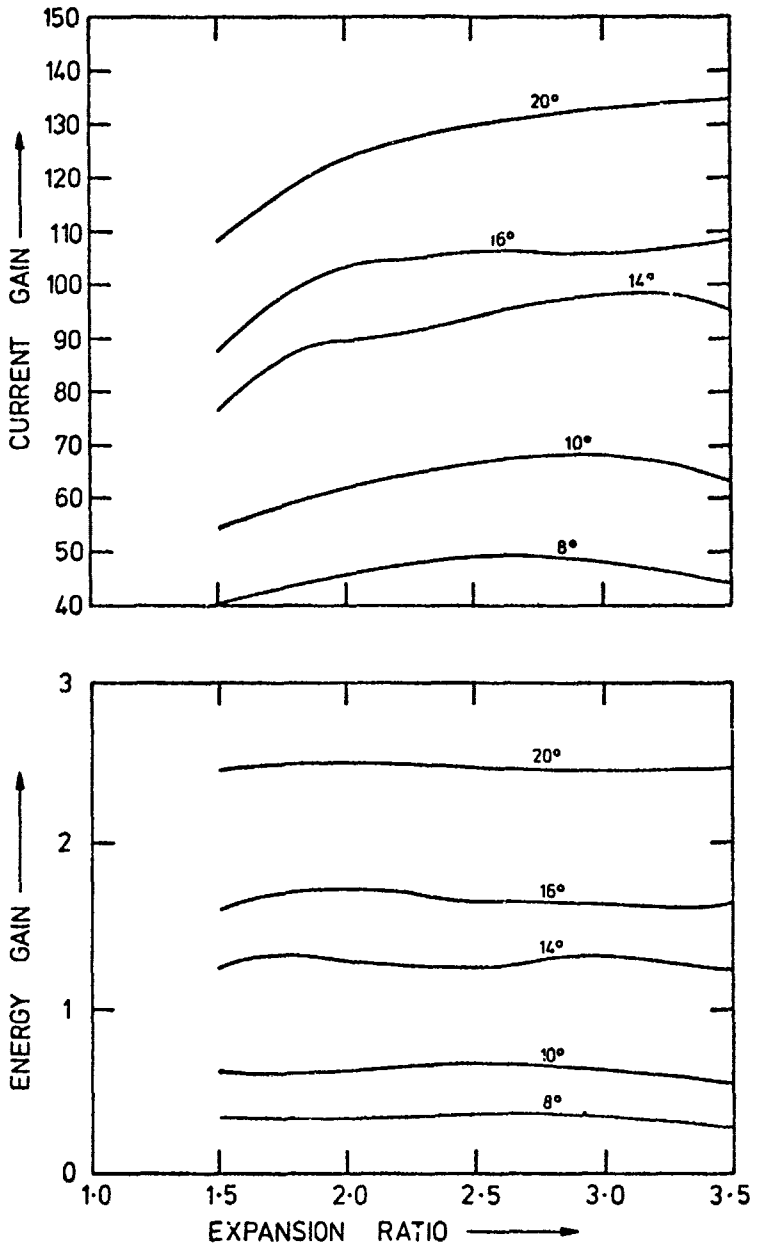

Fig 19

OUTPUT AS A FUNCTION OF
EXPANSION ANGLE AND EXPANSION RATIO

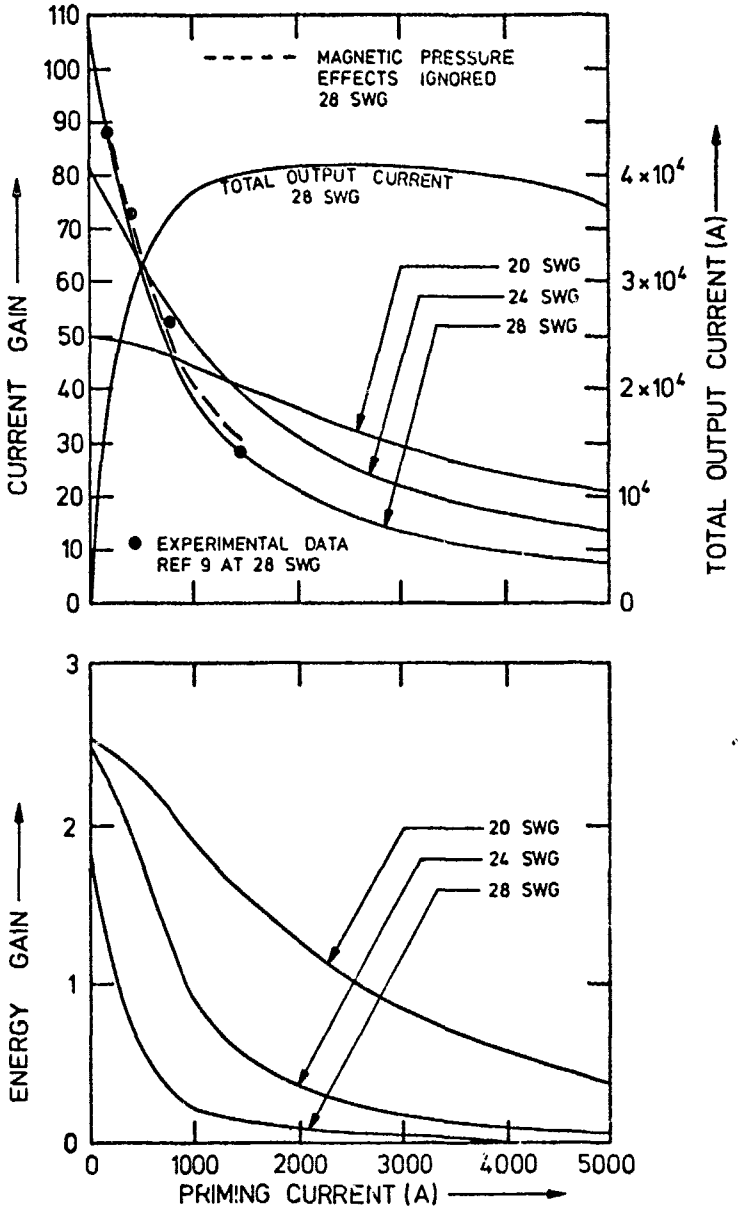

Fig 20

OUTPUT AS A FUNCTION OF
WIRE DIAMETER AND PRIMING CURRENT

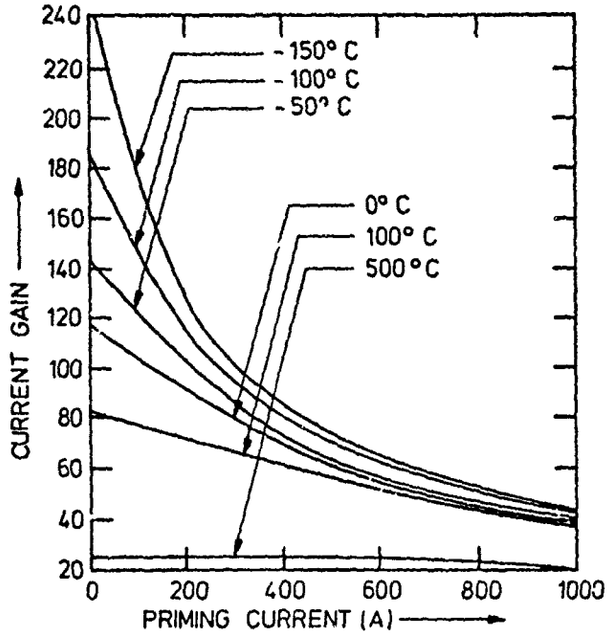

Fig 21
DIFFERING AMBIENT TEMPERATURES

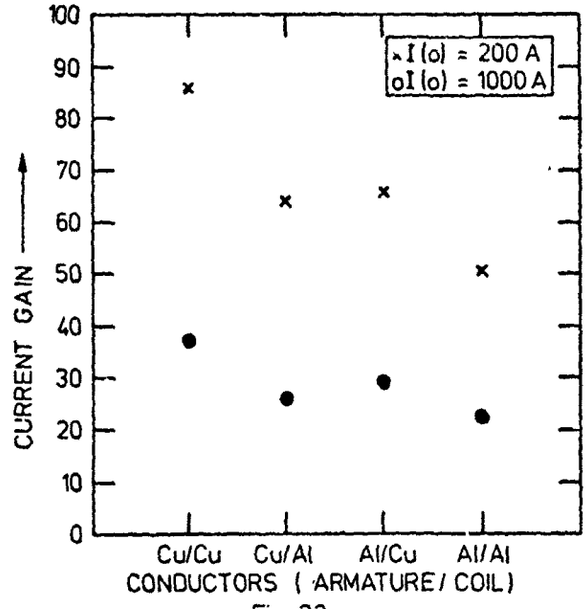

Fig 22
DIFFERING CONDUCTOR MATERIALS

DOCUMENT CONTROL SHEET

Overall security classification of sheet UNCLASSIFIED

(As far as possible this sheet should contain only unclassified information. If it is necessary to enter classified information, the box concerned must be marked to indicate the classification eg (R), (C) or (S)).

1. DRIC Reference (if known)	2. Originator's Reference	3. Agency Reference	4. Report Security Classification
-	AWRE REPORT No. 021/80	-	UNLIMITED

5. Originator's Code (if known)	6. Originator (Corporate Author) Name and Location
-	Atomic Weapons Research Establishment, Aldermaston, Berkshire

5a. Sponsoring Agency's Code (if known)	6a. Sponsoring Agency (Contract Authority) Name and Location
-	-

7. Title

Modelling of Compressed Magnetic Field Generators by Equivalent Circuit Approach

7a. Title in Foreign Language (in the case of Translation)

-

7b. Presented at (for Conference Papers). Title, Place and Date of Conference

-

8. Author 1.Surname, Initials	9a. Author 2	9b. Authors 3, 4	10. Date	pp	ref
Jones M	-	-	July 1980	51	9

11. Contract Number	12. Period	13. Project	14. Other References
-	-	-	-

15. Distribution Statement

No restrictions

16. Descriptors (or Keywords) (TEST)

Magnetic field compression
Explosive to electric energy
Transducers
Computer model

Abstract

An equivalent circuit model is presented for a helical compressed magnetic field generator. The emphasis has been placed on producing a model which has a short computer run time.

Magnetic energy losses due to non-linear field diffusion are taken into account, together with the effects of magnetically-induced conductor motion.

Examples of the computer code results are given, together with a comparison with experimental data.

Some Metric and SI Unit Conversion Factors

(Based on DEF STAN 00-11/2 "Metric Units for Use by the Ministry of Defence", DS Met 5501 "AWRE Metric Guide" and other British Standards)

Quantity	Unit	Symbol	Conversion
Basic Units			
Length	metre	m	1 m = 3.2808 ft 1 ft = 0.3048 m
Mass	kilogram	kg	1 kg = 2.2046 lb 1 lb = 0.45359237 kg 1 ton = 1016.05 kg
Derived Units			
Force	newton	$N = kg\ m/s^2$	1 N = 0.2248 lbf 1 lbf = 4.44822 N
Work, Energy, Quantity of Heat	joule	J = N m	1 J = 0.737562 ft lbf 1 J = 9.47817×10^{-4} Btu 1 J = 2.38846×10^{-4} kcal 1 ft lbf = 1.35582 J 1 Btu = 1055.06 J 1 kcal = 4186.8 J
Power	watt	W = J/s	1 W = 0.238846 cal/s 1 cal/s = 4.1868 W
Electric Charge	coulomb	C = A s	-
Electric Potential	volt	V = W/A = J/C	-
Electrical Capacitance	farad	F = A s/V = C/V	-
Electric Resistance	ohm	Ω = V/A	-
Conductance	siemen	$S = 1\ \Omega^{-1}$	-
Magnetic Flux	weber	Wb = V s	-
Magnetic Flux Density	tesla	$T = Wb/m^2$	-
Inductance	henry	H = V s/A = Wh/A	-
Complex Derived Units			
Angular Velocity	radian per second	rad/s	1 rad/s = 0.159155 rev/s 1 rev/s = 6.28319 rad/s
Acceleration	metre per square second	m/s^2	$1\ m/s^2 = 3.28084\ ft/s^2$ $1\ ft/s^2 = 0.3048\ m/s^2$
Angular Acceleration	radian per square second	rad/s^2	-
Pressure	newton per square metre	N/m^2 = Pa	$1\ N/m^2 = 145.038 \times 10^{-6}\ lbf/in^2$ $1\ lbf/in^2 = 6.89476 \times 10^3\ N/m^2$
	bar	bar = $10^5\ N/m^2$	- 1 in. Hg = 3386.39 N/m^2
Torque	newton metre	N m	1 N m = 0.737562 lbf ft 1 lbf ft = 1.35582 N m
Surface Tension	newton per metre	N/m	1 N/m = 0.0685 lbf/ft 1 lbf/ft = 14.5939 N/m
Dynamic Viscosity	newton second per square metre	$N\ s/m^2$	$1\ N\ s/m^2 = 0.0208854\ lbf\ s/ft^2$ $1\ lbf\ s/ft^2 = 47.8803\ N\ s/m^2$
Kinematic Viscosity	square metre per second	m^2/s	$1\ m^2/s = 10.7639\ ft^2/s$ $1\ ft^2/s = 0.0929\ m^2/s$
Thermal Conductivity	watt per metre kelvin	W/m K	-
Odd Units*			
Radioactivity	becquerel	Bq	1 Bq = 2.7027×10^{-11} Ci 1 Ci = 3.700×10^{10} Bq
Absorbed Dose	gray	Gy	1 Gy = 100 rad 1 rad = 0.01 Gy
Dose Equivalent	sievert	Sv	1 Sv = 100 rem 1 rem = 0.01 Sv
Exposure	coulomb per kilogram	C/kg	1 C/kg = 3876 R 1 R = 2.58×10^{-4} C/kg
Rate of Leak (Vacuum Systems)	millibar litre per second	mb l/s	1 mb = 0.750062 torr 1 torr = 1.33322 mb

*These terms are recognised terms within the metric system.